Revue des Composites et des Matériaux Avancés-Journal of Composite and Advanced Materials
Vol. 35, No. 6, December, 2025, pp. 1211-1216
Journal homepage: http://iieta.org/journals/rcma

Effect of Decoration $AgNO_3$ - $BaTiO_3$ Nanoparticles on the Structure and Optical Properties of PVA/PEO Polymer Blend

Zahraa A. Nayyef*, Abdulazeez O. Mousa Al-Ogaili, Ameerah Ab. Al-Sadooni

Department of Physics, College of Science, University of Babylon, Babylon 51001, Iraq

Corresponding Author Email: sci618.zahraa.ali@uobabylon.edu.iq

https://doi.org/10.18280/rcma.350620

Received: 17 November 2025
Revised: 18 December 2025
Accepted: 26 December 2025
Available online: 31 December 2025

Keywords:
PVA, PEO, $AgNO_3$, $BaTiO_3$, nanocomposite, crystallinity, surface plasmon resonance, XRD, FTIR, UV

ABSTRACT

This study investigates the effect of nanoparticles, namely silver nitrate ($AgNO_3$) and barium titanate ($BaTiO_3$), on polyvinyl alcohol (PVA)/ polyethylene oxide (PEO) blends prepared by casting at different weight ratios. Improving the structural and optical properties of polymer blends by incorporating nanoparticles is an important strategy for obtaining materials with advanced functions. X-ray diffraction (XRD) results confirm the semicrystalline nature of the pure polymer blend, the best peak was obtained at 2θ = 19.58°, with high-intensity other peaks at 2θ = 22.1° and 23.69°, which increased in crystallinity after the addition of nanoparticles due to the formation of distinct new crystalline phases at 2θ =19.61°, 22.4°, 23.59°, 19.4°, 23.46°, 23.51°, 31.92°, 39.25°, 47.74°, 50.94°, 56.48°, 65.71°, 54.61°, 31.65°, 39.03°, 45.15°, 56.29°, and 65.96°. Fourier transform infrared (FTIR) spectroscopy revealed distinct peaks at: 2884 cm^{-1} (C–H and C-O vibration in PEO/PVA), a broad band at 3300 to 3500 cm^{-1} (O–H groups, more in PVA), 1340.73 cm^{-1} (N–O vibration of $AgNO_3$), and 606.30 cm^{-1} (Ti–O bond of $BaTiO_3$). UV measurement results show that Pure PVA/PEO polymers blend absorb in the UV region 190 to 250 nm, and the addition of nanoparticles increases the absorption intensity between 300 and 600 nm.

1. INTRODUCTION

The PVA and PEO polymers are important materials in industrial [1], medical [2], and electronics applications due to their distinctive properties, such as water solubility, thermal stability, and ease of molding [3, 4], PVA and PEO polymers have also been used as carrier for nano materials, enabling other applications such as coatings, paints, and water treatment systems [5-7]. However, these polymers suffer from deficiencies in crystalline structure [8] and optical properties [9], which limits their effectiveness in advanced applications. Therefore, improving the crystallinity, optical, and functional properties of these polymers represents an important research challenge.

Recently, metallic nanoparticles such as $AgNO_3$ and $BaTiO_3$ have gained increasing importance due to their nanoscale dimensions, large specific surface area, and surface energy sites, which give them unique capabilities to interact with polymeric matrices [10]. Bimetallic nanoparticles consist of two different metallic elements, and of increasing importance due to their unique structure, which can be in the form of random alloys, intermetallic compounds, or core-and-shell structures, these give them enhanced properties compared to monometallic nanoparticles [11]. Given their size range (1-100) nm, their physical and chemical properties on this scale open up broad prospects for scientific and technological applications [12].

In the current study, the addition of $AgNO_3$ and $BaTiO_3$ to the selected polymers increased the degree of crystallinity. The results of FTIR analysis showed the presence of interactions between the additives and the functional groups of the polymer, consistent with previous studies referenced in these studies [3, 13], confirming structural changes at the molecular level that improved the materials' optical and crystalline properties. Additionally, despite the several recent publications, this study utilized two types of nanomaterials to enhance polymer properties, resulting in a composite material suitable for various applications such as batteries, sensors, and smart membranes. The study employed an easy and environmentally friendly casting technique. The primary objective was to investigate the effect of nanoparticles on the structural and optical properties of polymer composites, specifically their impact on structural and optical characteristics.

2. MATERIALS

The important information related to the materials used that employ to prepare thin films is listed in Table 1.

Table 1. Chemical compositions and supplier information of the used materials

	Name	Chemical Symbol	Molecular Weight (g/mol)	Purity (%)	Properties	Manufactured Company
Polymers	PVA	$H–(–CH_2–CH(OH)–)_n–H$	14000	99	White powder, water soluble, organic	BDH chemicals Ltd poole England
	PEO	$H–(O–CH_2–CH_2)_n–OH$	3×10^6	98	White granular, water soluble, organic	Cheng Du Micxy Chemical Co., Ltd.
Nanomaterials	$AgNO_3$	$(AgNO_3)_n$	169.87	99.9	Transparent, water soluble, inorganic	East francis street, Ontario, California, USA
	$BaTiO_3$	$(BaTiO_3)_n$	233.19	99.9	White powder, water soluble inorganic	Research nanomaterials, Inc. 0112 Twig, Leaf Ln. Houston, TX 77084 USA

3. NANOCOMPOSITE THIN FILMS PREPARATION

The three nanocomposite membranes were prepared using a single technique. This technique was followed to first prepare the required weight ratios of the materials for each of the three samples, as shown in Table 2. The second stage was to dissolve the required weights of PVA and PEO in deionized water (H_2O) using a Stewart magnetic stirrer with a moving speed of approximately 40 revolutions in minute at room temperature 22℃ for 1.5 hours until a completely homogeneous solution was obtained. The polymer solution was then poured into a 5 cm diameter plastic Petri dish and left to dry for 10 days in an isolated place from dust and impurities. The first sample (Zo) used 0.80 g of PVA and 0.20 g of PEO, resulting in a transparent film.

The sample Z1 used the same weight ratio of PVA, 0.170 g of PEO, and 0.015 g of $AgNO_3$ and $BaTiO_3$. The final sample Z2 used the same weight ratio of PVA, 0.155 g of PEO, 0.015 g of $AgNO_3$, and 0.030 g of $BaTiO_3$. The thicknesses of the resulting films were measured by using micro printer, ranging from 94 μm to 100 μm. Where the particle size ranges between (56.85-94.58) nm for Zo, (22.39-50) nm for Z1, and (24.76-41.21) nm for Z2.

Table 2. The weight percentages for each sample

Sample	PVA	PEO	$AgNO_3$	$BaTiO_3$
Zo	0.80	0.20	0	0
Z1	0.80	0.170	0.015	0.015
Z2	0.80	0.155	0.015	0.030

4. INSTRUMENTATIONS

The weight ratios were measured by using (KERN Cerman Company). The X-ray diffractometer type was used to investigate the crystal structure nature (Aeris-Malvern Panalytical device) current = 7.5 KV, wavelength = 1.54 Å. The optical FTIR analysis of the samples were measured using (B-ruker German company, type vertex-70 device). The UV/V is checked using a Shimadzu spectrometer.

5. RESULTS AND DISCUSSION

5.1 XRD analysis

Figure 1 presents the XRD patterns of pure PVA/PEO blend and the PVA, PEO, $AgNO_3$ and $BaTiO_3$ nanocomposite. The spectrum of pure PVA/PEO blend shows typical semicrystalline behavior, with three strong peaks at 2θ = 19.58°, 22.1° and 23.59°. The diffraction peaks observed correspond to the (040, 133 and 133) crystal structures of PVA/PEO polymers as indicated by standard reference patterns as shown in Figure 1(a). Additionally, smaller peaks appear at higher angles of 27°, 36°, and 39°, further supporting the concept that the polymers contain of both crystalline and non-crystalline regions. The broadening of these peaks in the polymers diffraction pattern suggests that the polymer exhibits a linear semicrystalline structure. This structural characteristic is crucial for stabilizing both chemically and electrochemically. The crystallization process in such polymers typically occurs through hierarchical organization across multiple length scales. During this process, the bending of polymer chains results in the formation of unique folded-chain layers that exhibit a specific molecular pattern. This chain-folding arrangement permits unconstrained expansion in two lateral dimensions. However, there is a limitation on the propagation of chain extension, with most defects concentrated at the folding surfaces. This finding is consistent with previous studies [14, 15].

In Figure 1(b), three strong peaks at 2θ = 19.61°, 22.4°, and 23.69° observed correspond to the (111, 102 and 020) crystal structures of PVA/PEO polymers. Additional peaks were also observed as a result of the addition of nanomaterials $AgNO_3$ and $BaTiO_3$. Peaks at 2θ = 31.92°, 39.25° and 47.74° correspond to the (113, 213 and 133) crystal structures of $AgNO_3$, the Bragg angle of $AgNO_3$ nanoparticles in the nanocomposites agrees with JCPDS data (Code 96-150-9469), peaks at 2θ = 31.92°, 50.94°, 56.48° and 65.71° correspond to the (113, 041, 240 and 151) crystal structures of $BaTiO_3$, the Bragg angle of $BaTiO_3$ nanoparticles agrees with JCPDS data (Code 96-152-5438).

Figure 1(c) shows peaks at 2θ = 19.4°, 23.46° and 23.51° observed correspond to the (011, 100 and 100) crystal structures of PVA/PEO. Peaks at 2θ = 31.65°, 39.03°, and 54.61° correspond to the (111 and 120) crystal structures of $AgNO_3$, and peaks at 2θ = 31.65°, 39.03°, 45.15°, 56.29°, and 65.96° correspond to the (111, 120, 022, 202, and 222) crystal structures of $BaTiO_3$ this behavior is similar to that presented by these studies [16, 17]. In summary, the XRD results show that adding more nanoparticles to the PVA/PEO matrix causes the peaks in the diffraction pattern to spread out more. This phenomenon can be attributed to structural modifications within the polymer matrix, which may stem from changes in the degree of crystallinity of polymers, shifts in polymer chain packing due to the incorporation of nanoparticles. From the X-ray diffraction (XRD) peaks, a number of structural parameters can be extracted to better understand the properties of the samples, where the interplanar d-spacing (*d*) is

calculated using the Bragg Eq. (1) [18]:

$$n\lambda = 2dsin(\theta) \quad (1)$$

where, n, λ, and θ mean the integer, wavelength, and angle of the X-ray between the incident and scattering beam, respectively. Meanwhile, the crystallite size (D) is calculated by applying the Scherrer Eq. (2) [19]:

$$D = k\lambda \,/\, \beta cos(\theta) \quad (2)$$

where, k = ~0.9 is the factor of the crystals mean and β the full width at half the maximum peak (FWHM), as exposed in Table 3. The lattice strain ($\mathcal{E}$) is measured by using Eq. (3) [19]:

$$\varepsilon = \beta \,/\, 4tan(\theta) \quad (3)$$

The crystallite size (D) of samples was impacted and increased with adding the nanoparticles in polymer blend. The results show that the PVA/PEO polymer blend has a semi-crystalline nature with amorphous regions, while the introduction of nanomaterials $AgNO_3$ and $BaTiO_3$ contributed to the appearance of new peaks and increased the intensity of some crystalline peaks, indicating enhanced crystallinity and improved crystal structure of the sample. Table 3 contains important parameters for these films, intensity, distance between crystal planes, and full width at half maximum, crystallite size, and lattice strain.

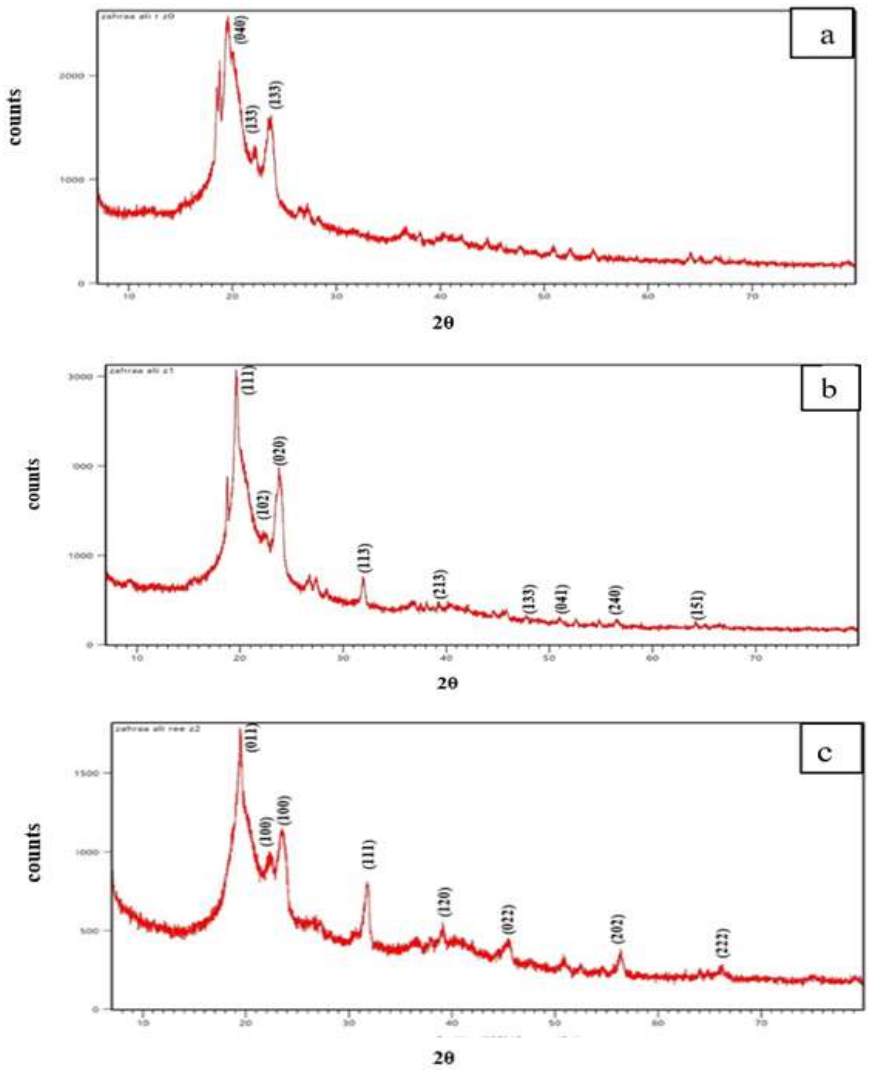

Figure 1. XRD analyses of (a) PVA / PEO polymers blend for Zo, (b) PVA/PEO, $AgNO_3$ and $BaTiO_3$ nanocomposite for Z1 and (c) PVA/PEO, $AgNO_3$ and $BaTiO_3$ nanocomposite for Z2

Table 3. X-ray parameters for polymers and nanomaterials of prepared thin films

Sample		2θ (deg)	Intensity (count/s)	(hkl)	d-Spasing (Å)	FWHM (deg)	Crystallite Size (Å)	Lattice Strain ($\mathcal{E}$)
Zo	PVA	22.1	1295.97	(133)	3.998	1.008	45	4.43
	PEO	19.58	2543.89	(040)	4.530	1.454	31	7.27
		23.59	1489	(133)	3.768	0.877	74	2.55
Z1	PVA	22.4	1234.36	(102)	3.953	0.914	63	3.15
	PEO	19.61	372.6	(111)	4.521	0.739	62	3.63
		23.69	1817.72	(020)	3.751	0.716	122	1.53
	$AgNO_3$	31.92	744.24	(113)	2.801	0.370	199	0.7

		39.25	459	(213)	2.293	0.213	444	0.25
		47.74	315.89	(133)	1.903	0.197	365	0.26
		31.92	744.24	(113)	2.801	0.370	199	0.7
	$BaTiO_3$	50.94	308.76	(041)	1.791	0.258	232	0.38
		56.48	265.42	(240)	1.627	0.468	123	0.66
		65.71	212.42	(151)	1.419	7.412	7	10.22
	PVA	23.51	1116.42	(100)	3.787	1.001	60	3.14
	PEO	19.4	1639.55	(011)	4.571	0.823	55	4.12
		23.46	1116.42	(100)	3.787	1.001	60	3.14
	$AgNO_3$	31.65	743.78	(111)	2.824	0.706	81	1.74
Z2		39.03	489.87	(120)	2.305	0.863	55	2.08
		31.65	743.78	(111)	2.824	0.706	81	1.74
		39.03	489.87	(120)	2.305	0.863	55	2.08
	$BaTiO_3$	45.15	409.26	(022)	2.006	1.847	26	3.84
		56.29	340.55	(202)	1.632	0.574	142	0.57
		65.96	248.35	(222)	1.414	1.768	33	2.12

5.2 FTIR analysis

The main functions of using FTIR are to assess the type of chemical bonding between the different phases, and to examine whether there is a chemical reaction or just physical mixing, and to qualitatively analyze the materials present in the bulk of the films [20]. The FTIR analysis of PVA, PEO, $AgNO_3$ and $BaTiO_3$ films in the frequency region of 400 to 4000 cm^{-1} was examined as illustrated in Figure 2. In Figure 2(a), blended polymers spectrum exhibited strong absorption peaks at 1096.62 cm^{-1} and 2884 cm^{-1} corresponds to the C-O and C-H bending vibrations, respectively, of the polymers. Broad peak between 3500 to 3300 cm^{-1} corresponds to the O–H bending vibrations and this behavior is similar to that presented by Abdali et al. [21]. In Figure 2(b), another new absorption peak located at 1340.73 cm^{-1} was associated with the N-O stretching vibration of $AgNO_3$. $BaTiO_3$ does not appear directly here because most of its vibrations appear in the very low infrared region, which may not be visible here. In Figure 2(c), other new absorption peak located at 606.30 cm^{-1} were associated with Ti-O stretching vibration of $BaTiO_3$ and this behavior is similar to that presented by Soliman et al. [22]. The peaks specific to PVA and PEO remain, indicating that the basic structure of the polymers is preserved. The increased appearance of new peaks and changes in intensity are evidence of an interaction between nanoparticles and polymer functional groups.

5.3 Ultraviolet and visible analysis UV/Vis

The absorption spectrum was, measured using a dual-beam (UV-Visible - Spectrophotometer) this spectrometer, covers a wide area of the electromagnetic spectrum from the, ultraviolet region to the near-infrared region range of 190 to 1100 nm. UV-Vis spectroscopy measures the attenuation of a light beam after it passes through or is reflected from a sample. Figure 3 presents the absorption spectra of both pure PVA/PEO blend and the PVA, PEO, $AgNO_3$ and $BaTiO_3$ nanocomposite.

The pure polymers blend spectrum has a noticeable absorption peak between 190 to 250 nm and is due to electronic transitions $n \rightarrow \pi^*$, indicating absorption in the far-ultraviolet region. Upon incorporation of $AgNO_3$ and $BaTiO_3$ nanoparticles into the PVA/PEO matrix, a substantial rise in absorbance across the UV-Vis range is observed 300 to 450 nm. These absorptions for nanoparticles appear peaks at 420 nm. This is evidenced by an elevated absorption coefficient, suggesting a transition toward longer wavelengths. Silver nanoparticles exhibit distinct absorption due to the surface plasmon resonance (SPR) phenomenon in the range 400 to 450 nm. The concentration value has a high impact on the absorption spectrum which increases upon higher concentration value [23].

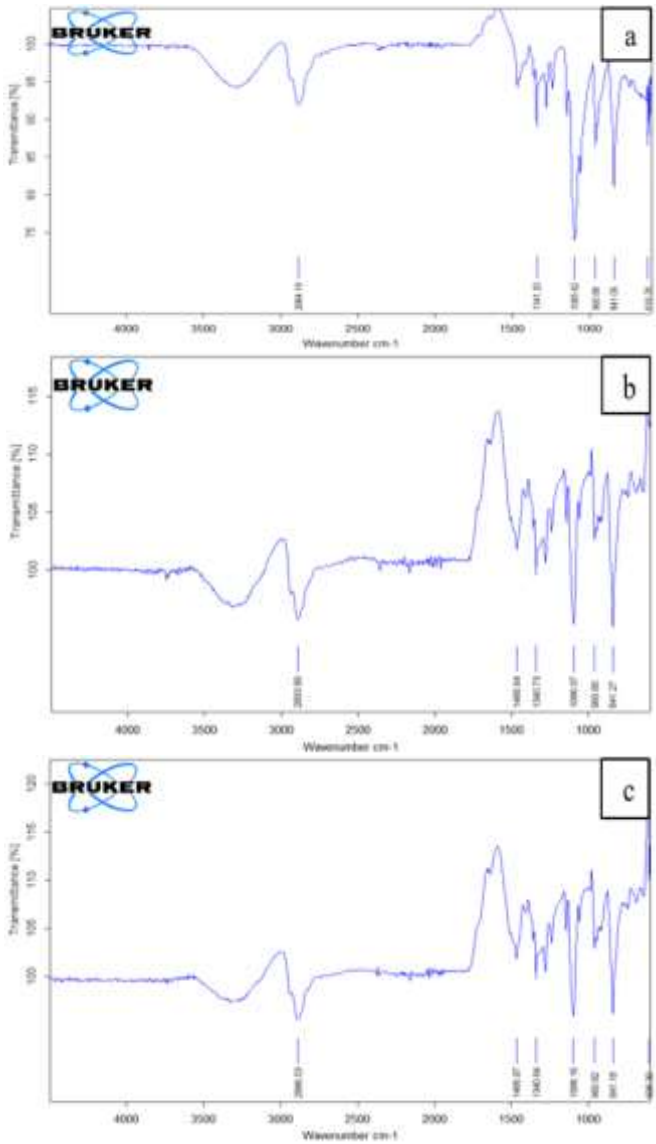

Figure 2. FTIR spectra of (a) PVA / PEO polymers blend for Zo, (b) PVA / PEO, $AgNO_3$ and $BaTiO_3$ nanocomposite for Z1 and (c) PVA / PEO, $AgNO_3$ and $BaTiO_3$ nanocomposite for Z2

In general, samples containing nanoparticles show a clear increase in absorption between 300 to 600 nm. This is due to

absorb the incident light by free electrons, then the absorption of samples Z1 and Z2, stabilizes at higher wavelengths compared to sample Zo. The absorption coefficient (α_o) is defined as a measure of the rate of decrease in the energy of the incident electromagnetic radiation per unit length along the direction of wave propagation within the material medium and is given by Eq. (5) [24]:

$$Log(I/Io) = 2.303A = \alpha od \quad (4)$$

$$\alpha o = 2.303\frac{A}{d} \quad (5)$$

where, I represents the intensity of the electromagnetic radiation (light) before entering the sample, Io the intensity of light after passing through the sample, d the thickness, and A is the absorbance.

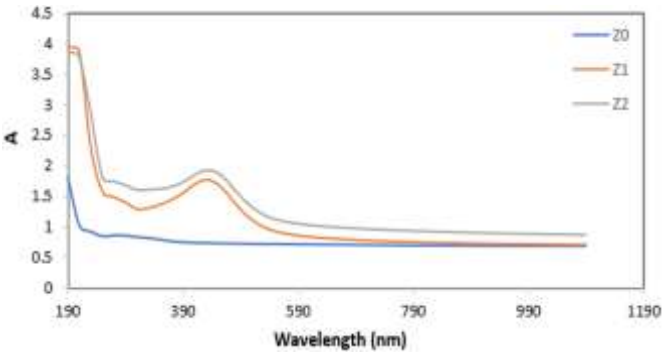

Figure 3. Absorbance spectra of (Z_O) PVA/PEO blend, and (Z1)(Z2) PVA, PEO, $AgNO_3$ and $BaTiO_3$ nanocomposite thin films

3. CONCLUSIONS

The results of the study revealed that the incorporating of $AgNO_3$ and $BaTiO_3$ nanoparticles into a PVA/PEO polymer matrix significantly enhances the degree of crystalline ordering, resulting in the formation of semi-crystalline thin films characterized by improved structural properties. XRD analysis shown best peak that was at $2\theta = 19.58°$ due to the diffraction reflection from the distinct crystal planes of the polymer lattice, it indicates that it contains crystalline regions in addition to amorphous regions with high-intensity other peaks at $2\theta = 22.1°$ and 23.0° of pure polymers. New peaks appeared at $2\theta = 31.92°$, 39.25°, 47.74°, 56.48°, and 65.71° after the addition of $AgNO_3$ and $BaTiO_3$, reflecting increased crystallinity. Corresponding crystal planes were identified, such as (040, 133, 111, 113, 120, 151), and others, strengthening the evidence of a regular structure, and decrease in lattice strain was observed after adding nanoparticles to the polymer matrix. This is attributed to the improved crystallization process; the integration of nanomaterials into a polymer matrix enhances crystallinity due to several interrelated factors. Most importantly, nanomaterials act as nucleating agents, possessing a very high surface area that provides readily available sites for crystal growth within the polymer. Additionally, the presence of nanomaterials within the polymer can guide the chains, forcing them into a more ordered arrangement. This organization facilitates the transition of the chains from an amorphous to a crystalline state, limiting the formation of crystal defects and contributing to increased crystal lattice regularity.

FTIR analysis revealed absorption peaks at 2884 cm^{-1} for the C–H group, 3500 to 3300 cm^{-1} for the O–H group, and 1096.62 cm^{-1} for the PEO group, in addition to peaks associated with $AgNO_3$ at 1340.73 cm^{-1}, and a distinct peak for $BaTiO_3$ at 606.30 cm^{-1}, attributed to the Ti–O bond. The absence of new bonds indicates that the mixing was physical, while the chemical compositions of the polymers were preserved. These findings indicate that the synthesized materials possess promising potential for applications in flexible electronics, sensors, biomedical films, and energy storage systems, owing to their optimized balance between crystallinity, flexibility, and structural stability. The increased appearance of new peaks and changes in intensity are evidence of an interaction between nanoparticles and polymer functional groups.

The UV-Vis data indicate that the incorporation of $AgNO_3$ and $BaTiO_3$ nanoparticles into the polymer matrix significantly alters the light absorption behavior compared to pure polymers. The absorption of the Zo sample is limited to electronic transitions in the ultraviolet range, while $BaTiO_3$ adds a broader absorption range extending into visible light, reflecting its ability to interact with high-energy photons. The appearance of a sharp peak at 420 nm confirms the formation of functional silver nanoparticles with surface plasmon resonance (SPR). The increase in absorption with increasing nanoparticle concentration demonstrates that the particle density and number of free electrons contribute to enhanced light absorption across the 300 to 600 nm range. It can therefore be concluded that the incorporation of nanoparticles improves the optical absorption properties of polymers, making these materials candidates for optical or photonic applications such as sensors or photoresistors in the visible range. The same nanomaterials, either both materials or a single material combined with new polymers, can be used in future work.

ACKNOWLEDGMENT

The authors would like to acknowledge the colleagues and professors from the Department of Physics at the University of Babylon for their guidance and valuable insights during the composition of this study. And to acknowledge and appreciate also Dr. Abdali, K., and Dr. Huda Raad for their assistance.

REFERENCES

[1] Mark, J. (1999). Polymer Data Handbook. New York: Oxford University Press.

[2] Latif, D.M., Chiad, S.S., Erhayief, M.S., Abass, K.H., Habubi, N.F., Hussin, H.A. (2018). Effects of $FeCl_3$ additives on optical parameters of PVA. Journal of Physics: Conference Series, 1003(1): 012108. https://doi.org/10.1088/1742-6596/1003/1/012108

[3] Al-jamal, A.N., Hadi, Q.M., Hamood, F.J., Abass, K.H. (2019). Particle size effect of Sn on structure and optical properties of PVA-PEG blend. In 2019 12th International Conference on Developments in eSystems Engineering (DeSE), Kazan, Russia, pp. 736-740. https://doi.org/10.1109/DeSE.2019.00137

[4] Sharba, K.S., Alkelaby, A.S., Sakhil, M.D., Abass, K.H., Habubi, N.F., Chiad, S.S. (2020). Enhancement of

urbach energy and dispersion parameters of polyvinyl alcohol with Kaolin additive. NeuroQuantology, 18(3): 66-73. https://doi.org/10.14704/nq.2020.18.3.NQ20152
[5] Kumar, A., Vemula, P.K., Ajayan, P.M., John, G. (2008). Silver-nanoparticle-embedded antimicrobial paints based on vegetable oil. Nature Materials, 7(3): 236-241. https://doi.org/10.1038/nmat2099
[6] Oyanedel-Craver, V.A., Smith, J.A. (2008). Sustainable colloidal-silver-impregnated ceramic filter for point-of-use water treatment. Environmental Science & Technology, 42(3): 927-933. https://doi.org/10.1021/es071268u
[7] Pal, S., Yoon, E.J., Tak, Y.K., Choi, E.C., Song, J.M. (2009). Synthesis of highly antibacterial nanocrystalline trivalent silver polydiguanide. Journal of the American Chemical Society, 131(44): 16147-16155. https://doi.org/10.1021/ja9051125
[8] Menazea, A.A. (2020). One-pot pulsed laser ablation route assisted copper oxide nanoparticles doped in PEO/PVP blend for the electrical conductivity enhancement. Journal of Materials Research and Technology, 9(2): 2412-2422. https://doi.org/10.1016/j.jmrt.2019.12.073
[9] Ghazi, R.A., Al-Mayalee, K.H., Al-Bermany, E., Hashim, F.S., Albermany, A.K.J. (2022). Impact of polymer molecular weights and graphene nanosheets on fabricated PVA-PEG/GO nanocomposites: Morphology, sorption behavior and shielding application. AIMS Materials Science, 9(4): 584-603. https://doi.org/10.3934/matersci.2022035
[10] Abdali, K. (2022). Synthesis, characterization and USW sensor of PEO/PMMA/PVP doped with zirconium dioxide nanoparticles. Transactions on Electrical and Electronic Materials, 23(5): 563-568. https://doi.org/10.1007/s42341-022-00388-7
[11] Alawi, A.I., Al-Bermany, E. (2023). Newly fabricated ternary PAAm-PVA-PVP blend polymer doped by SiO_2: absorption and dielectric characteristics for solar cell applications and antibacterial activity. Silicon, 15(13): 5773-5789. https://doi.org/10.1007/s12633-023-02477-5
[12] Kadhim, A.A., Al-Ogaili, A.O.M., Abass, K.H. (2022). Effect of adding silver nanoparticles on structural and microscopic properties of PAAm-PEG polymer blend. Journal of Nanostructures, 12(4): 892-897. https://doi.org/10.22052/JNS.2022.04.011
[13] Blosi, M., Ortelli, S., Costa, A.L., Dondi, M., et al. (2016). Bimetallic nanoparticles as efficient catalysts: Facile and green microwave synthesis. Materials, 9(7): 550. https://doi.org/10.3390/ma9070550
[14] Xu, L., Wei, K., Cao, Y., Ma, S., et al. (2020). The synergistic effect of the PEO–PVA–PESf composite polymer electrolyte for all-solid-state lithium-ion batteries. RSC Advances, 10(9): 5462-5467. https://doi.org/10.1039/c9ra09645k
[15] Hassan, A.A., Al-Ogaili, A.O.M. (2025). The impact of psyllium husk Addition on the some physical properties of PEO polymer. Journal of Composite & Advanced Materials/Revue des Composites et des Matériaux Avancés, 35(1): 71-79. https://doi.org/10.18280/rcma.350109
[16] Saini, I., Rozra, J., Chandak, N., Aggarwal, S., Sharma, P.K., Sharma, A. (2013). Tailoring of electrical, optical and structural properties of PVA by addition of Ag nanoparticles. Materials Chemistry and Physics, 139(2-3): 802-810. https://doi.org/10.1016/j.matchemphys.2013.02.035
[17] Beena, P., Jayanna, H.S. (2019). Dielectric studies and AC conductivity of piezoelectric barium titanate ceramic polymer composites. Polymers and Polymer Composites, 27(9): 619-625. https://doi.org/10.1177/0967391119856140
[18] Yang, Z., Zhang, Y., Wen, B. (2019). Enhanced electromagnetic interference shielding capability in bamboo fiber@ polyaniline composites through microwave reflection cavity design. Composites Science and Technology, 178: 41-49. https://doi.org/10.1016/j.compscitech.2019.04.023
[19] Qiu, M., Zhang, Y., Wen, B. (2018). Facile synthesis of polyaniline nanostructures with effective electromagnetic interference shielding performance. Journal of Materials Science: Materials in Electronics, 29(12): 10437-10444. https://doi.org/10.1007/s10854-018-9100-6
[20] Muheddin, D.Q., Aziz, S.B., Mohammed, P.A. (2023). Variation in the optical properties of PEO-based composites via a green metal complex: Macroscopic measurements to explain microscopic quantum transport from the valence band to the conduction band. Polymers, 15(3): 771. https://doi.org/10.3390/polym15030771
[21] Abdali, K., Abass, K.H., Al-Bermany, E., Al-robayi, E.M., Kadim, A.M. (2022). Morphological, optical, electrical characterizations and anti-Escherichia coli bacterial efficiency (AECBE) of PVA/PAAm/PEO polymer blend doped with silver NPs. Nano Biomedicine & Engineering, 14(2): 114-122. https://doi.org/10.5101/nbe.v14i2.p114-122
[22] Soliman, T.S., Zaki, M.F., Hessien, M.M., Elkalashy, S.I. (2021). The structure and optical properties of PVA-$BaTiO_3$ nanocomposite films. Optical Materials, 111: 110648. https://doi.org/10.1016/j.optmat.2020.110648
[23] Bhalla, N., Shen, A.Q. (2024). Localized surface plasmon resonance sensing and its interplay with fluidics. Langmuir, 40(19): 9842-9854. https://doi.org/10.1021/acs.langmuir.4c00374
[24] Lazzeretti, P. (2019). Continuity equations for electron charge densities and current densities induced in molecules by electric and magnetic fields. The Journal of Chemical Physics, 151(11): 114108. https://doi.org/10.1063/1.5124250